

# An Individual Tree Segmentation Method Based on Watershed Algorithm and Three-Dimensional Spatial Distribution Analysis From Airborne LiDAR Point Clouds

Juntao Yang<sup>✉</sup>, Zhizhong Kang<sup>✉</sup>, Sai Cheng, Zhou Yang, and Perpetual Hope Akwensi<sup>✉</sup>

**Abstract**—Accurate individual tree segmentation is an important basis for the subsequent calculation and analysis of forestry parameters. However, rasterized canopy height model based methods often suffer from 3-D information loss due to the interpolation operation. Therefore, this article proposes an individual tree segmentation method based on the marker-controlled watershed algorithm and 3-D spatial distribution analysis from airborne LiDAR point clouds. First, based on the potential tree apices derived from the local maxima filtering, the marker-controlled watershed segmentation algorithm is conducted to obtain the coarse point clusters. Then, within the principal component analysis defined local coordinate reference framework, a multidirectional 3-D spatial profile analysis is performed on each point cluster to refine the potential tree apex positions. Finally, the refined potential tree apex positions are used as a prior of K-means clustering to achieve the coarse-to-fine individual tree segmentation. Comparative experiments were conducted on the public NEWFOR dataset to evaluate the proposed method. Results indicate that the proposed method is efficient and robust for segmenting individual trees.

**Index Terms**—Airborne LiDAR, canopy height model (CHM), individual tree segmentation, profile analysis, watershed algorithm.

## I. INTRODUCTION

FOREST ecosystem, one of the largest and most important natural ecosystems among all the terrestrial ecosystems, is a natural complexity with specific structure, function, and self-regulation capability, formed by the forest community and its environment. Its primary characteristics are a variety of animal and plant species, and complicated community structures, where the population density and the community structures can be in a stable state for a long time, especially in the tropical

Manuscript received August 23, 2019; revised December 13, 2019 and January 7, 2020; accepted March 1, 2020. Date of publication March 12, 2020; date of current version April 3, 2020. This work was supported by the National Natural Science Foundation of China under Grant 41872207. (Corresponding author: Zhizhong Kang.)

The authors are with the School of Land Science and Technology, China University of Geosciences, Beijing 100083, China, and with the Subcenter of International Cooperation and Research on Lunar and Planetary Exploration, Center of Space Exploration, Ministry of Education of The People's Republic of China, Beijing 100083, China, and also with the Shanxi Key Laboratory of Resources, Environment and Disaster Monitoring, Jinzhong 030600, China (e-mail: jtyang66@126.com; zzkang@cugb.edu.cn; 18101361751@163.com; 15047137010@163.com; ahimeless@outlook.com).

Digital Object Identifier 10.1109/JSTARS.2020.2979369

rainforest ecosystem. Obviously, the forest ecosystem and its changes are of special ecological significance in maintaining the pattern, function, and process of the natural ecosystem [1]. Furthermore, the sustainable service capability of a forest is dependent on the efficient forest management and scientific understanding of carbon, water, and nutrient cycling [2]. As the basic unit of forest, the spatial structure, biophysics, and chemical composition of individual trees are the key factors for forest stock [3] and biomass estimation [4], species identification [5], [6], tree growth modeling [7] etc. Therefore, the automatic delineation of the individual trees has always been and still is one of the most critical topics in forest resource investigation and management.

Traditional forestry survey methods require manual field investigation over the whole forest area [8], which is time consuming, laborious, and difficult to obtain regional and large-scale data. At present, remote sensing techniques provide an effective substitute to the manual field survey. With the development of remote sensing technology, forest remote sensing has gradually developed from the early qualitative study, such as forest classification and mapping [9], to the quantitative analysis of the overall characteristics of forests [10]–[14]. Moreover, the individual tree information derived from remote sensing data can not only effectively improve the efficiency of forest survey but can also ensure the spatial integrity and temporal consistency of individual tree information with high accuracy.

Airborne laser scanning as a novel active remote sensing is a technology that can effectively support forest survey, research, and management. The use of LiDAR technologies in forest inventory has made it possible for forest stands to be measured at individual tree level [15]. LiDAR data, due to their high resolution, can be used to measure the horizontal and vertical structure of a forest stand. Furthermore, compared to other traditional remote sensing techniques, LiDAR has the ability to penetrate forest canopy thus enabling us to obtain more accurate digital elevation model, digital surface model (DSM), and canopy growth state, which in turn shows the potential and advantages of accurate estimation of forest parameters like individual tree height, forest floor topography, forest stand biomass, number of trees, and circumference of tree crown.

Although numerous individual tree segmentation methods have been developed in recent years, it is still challenging. For canopy height model (CHM) based methods, the CHM is generated through rasterization and interpolation techniques during which some part of the 3-D information in the raw point clouds often gets lost. At the same time, rasterization might smooth the original shape of the tree crown. Moreover, the grid size employed in the rasterization process is also an important factor, which affects the performance of the subsequent segmentation. More recently, point cloud-based methods are increasingly becoming popular and can directly detect the individual tree crowns by analyzing their spatial distribution, which eliminates the effect of information loss due to rasterization compared with CHM-based methods. Nevertheless, it is well known that point cloud-based method usually requires a lot of knowledge-based rules because of the unstructured nature of discrete point clouds, which might be not applicable.

To address these challenges, this article proposes a hybrid method, which combines the marker-controlled watershed algorithm and multidirectional 3-D spatial distribution analysis, to achieve a coarse-to-fine individual tree segmentation from airborne LiDAR point clouds. Furthermore, a qualitative and quantitative analysis is carried out on the public NEWFOR dataset [16] to evaluate the validity and robustness of the proposed method. The main contributions of the proposed method are as follows.

- 1) Considering the spatial distribution characteristics of multiple (overlapping) trees, a multidirectional 3-D spatial profile analysis within the principal component analysis (PCA) based local coordinate framework is carried out in 3-D space to refine the positions of the potential tree apices so as to effectively improve the performance of tree apex detection.
- 2) Based on the coarse segmentation derived from CHM, the refined potential tree apex positions are used as a prior of K-means clustering algorithm to realize the coarse-to-fine segmentation of single trees.

The rest of this article is organized as follows. Works related to the individual tree delineation are reviewed in Section II. Section III describes the proposed method in detail. Section IV presents the experimental results and analysis for evaluating the proposed method. This article concludes with a discussion of future research considerations in Section V.

## II. RELATED WORK

To date, LiDAR data-derived individual tree delineation has become a hot topic in forest remote sensing and numerous individual tree segmentation approaches have been proposed, which can be generally divided into two categories: CHM-based methods and point cloud-based methods.

### A. CHM-Based Methods

CHM-based methods mainly use current image segmentation techniques, such as template matching, region growing, or watershed-based methods, on a rasterized CHM derived from LiDAR point clouds using surface interpolation, to extract and

segment individual trees. Indeed, the key insight behind majority of the CHM-based methods is that a single tree has exactly one treetop and its tree crown exhibit a general ellipsoidal shape. Based on this assumption, the local maxima within a certain spacing can be considered as the position of the individual treetop. Koch *et al.* [17] conducted a knowledge-based individual tree crown detection after a local maximum filtering from rasterized LiDAR data in deciduous and mixed temperate forests. However, finding the local maxima largely depends on the determination of the window size, which might result in over-segmentation or under-segmentation. Considering the fact that there is a relationship between the tree height and the tree crown, Chen *et al.* [18] detected the treetops as markers via local maximum filtering with variable window sizes in a CHM and applied a marker-controlled watershed segmentation to isolate single trees. Unlike the work presented in [18], there are many approaches for alleviating this over-segmentation or under-segmentation. Mongus and Žalik [19] combined the treetops derived from the local maximum filter and tree trunks for optimizing the 3-D single tree crown delineation. Parkan and Tuia [20] modeled the uncertainty of coarse delineation derived from marker-controlled watershed segmentation with ensemble-based filtering for removing erroneous initial segmentation. Liu *et al.* [21] used crown boundary refinement based on a proposed fishing net dragging method and segment merging based on boundary classification to individually delineate tree crowns from airborne LiDAR data. To handle the symmetry of the citrus tree, Ok and Ozdarici-Ok [22] presented an original approach to detect and delineate citrus trees using unmanned aerial vehicle (UAV) based photogrammetric DSMs, where an orientation-based radial symmetry transform was performed and then the individual citrus trees were delineated using active contours. Similarly, Dong *et al.* [23] also developed an automated single tree detection framework based on gradient orientation clustering from rasterized airborne LiDAR point clouds. Pirotti [24] adopted a template matching method to extract a correlation map from LiDAR-derived digital CHM for obtaining stem density, position, and height values. Zaforemska *et al.* [25] investigated five existing individual tree detection methods and drew a conclusion that the rasterized CHM-based methods highly relied on the size of moving window used to detect the local maxima. Unlike the previous local maxima filtering methods, Holmgren and Lindberg [26] established a tree crown density model to represent the correlation surface, which served as the input of the conventional watershed segmentation algorithm for the tree crown delineation. However, this method requires the positions of individual trees as a prior. Marinelli *et al.* [27] developed a Bayesian fusion method to detect the trees from bitemporal LiDAR data.

### B. Point Cloud-Based Method

Currently, there are many methods based on point cloud distribution recognition, including voxel-based clustering methods, K-means clustering methods, Markov-based clustering methods, and global clustering methods. Morsdorf *et al.* [28] used treetops as a prior of K-means clustering approach for single

tree detection. Li *et al.* [29] segmented single tree crowns based on the relative spacing between trees. Yao *et al.* [30] conducted a sensitivity analysis of the parameters 3-D individual tree detection methods use, to guide the selection of parameter values in new applications. Lu *et al.* [31] studied the intensity and 3-D structure of leaf-off LiDAR point clouds and then developed an individual tree segmentation approach from tree trunks to other parts. Generally speaking, the position of an individual tree crown should be identical at several vertical neighboring layers. Based on this assumption, Wang *et al.* [32] analyzed projection images at different height levels, and implemented a clustering algorithm at each level to extract single trees. Similar to the work presented in [32], Ayrey *et al.* [33] also developed an automatic slice-based method, where whole point clouds were sliced into different layers and individual trees were delineated via intralayer isolation and interlayer merging of points. On the basis of the work presented in [32], Kandare *et al.* [34] mainly analyzed the effects of forest structure and point cloud density on the performance of 3-D delineation of individual tree crowns. Ferraz *et al.* [35] implemented the mean shift algorithm to decompose the airborne LiDAR point clouds into individual trees. Following the previous work [35], Dai *et al.* [36] investigated the performance of multispectral LiDAR for delineating individual trees using the mean shift algorithm, where both spatial and spectral information were used to refine the segmentation. Yan *et al.* [37] first carried out a voxel-based mean shift segmentation algorithm on a normalized nonground UAV LiDAR point cloud for 3-D single tree segmentation and then used normalized cut segmentation for optimizing the under-segmented parts. Xiao *et al.* [38] investigated the performance of mean shift algorithm and its variants for tree segmentation from airborne LiDAR data. Ramiya *et al.* [39] presented a super-voxel-based labeling framework for delineating individual trees from airborne LiDAR. Harikumar *et al.* [40] combined 3-D volumetric texture and 2-D crown boundary to detect both dominant and subdominant tree crowns from high-density airborne LiDAR data.

To sum up, CHM-based methods generally formulate the individual tree detection into a gray-scale image segmentation problem, and numerous well-established image segmentation techniques can be applied for achieving the superior performance. Unavoidably, the performance of these CHM-based methods is limited by the spatial interpolation and rasterization processes since 3-D information can successfully provide important factors from another perspective for effective individual tree segmentation. In comparison with the CHM-based methods, the point cloud-based methods directly are implemented on 3-D point clouds without any information loss. Due to the inherent characteristics of 3-D point clouds (such as being unstructured, discrete, uneven), these point cloud-based methods generally require certain complicated knowledge-based assumptions.

### III. METHODOLOGY

It is well known that for majority of the CHM-based methods, the performance largely depends on the effectiveness and robustness of the local maxima filter. Hence, we present an

individual tree segmentation method based on the marker-controlled watershed algorithm and a 3-D spatial distribution analysis from airborne LiDAR point clouds. Fig. 1 shows the workflow of the proposed method. It consists of two parts: 2-D CHM-based coarse segmentation and 3-D point cloud-based fine segmentation. Referring to the previous work [18], the coarse tree segmentation is performed on a rasterized CHM. Based on the CHM-derived coarse segmentation, a multidirectional 3-D spatial profile analysis is carried out through the local maximum shape curve fitting to refine the potential tree apex positions, which serves as the initial seeds of K-means clustering algorithm. As a result, the raw point clouds are segmented into a set of individual trees. Key algorithms of our proposed method are given in detail below.

#### A. Two-Dimensional CHM-Based Coarse Segmentation

As mentioned earlier, after transforming the 3-D point cloud into CHM, the single tree detection based on CHM is formulated into a gray-scale image segmentation problem, in which many well-established image segmentation methods (e.g., region growing method, watershed algorithm, and template matching) have been successfully applied. However, the traditional watershed segmentation algorithm always produces over-segmentation issues due to noises. To solve the over-segmentation issues from numerous potentials but trivial regional minima, marker-controlled watershed segmentation as a variant of the classical watershed segmentation [41] has been proposed and successfully used in single tree detection applications. Thus, in this section, we conduct a marker-controlled watershed segmentation [42] for 2-D CHM-based coarse segmentation, which includes CHM generation and coarse segmentation via a marker-controlled watershed segmentation.

1) *CHM Generation*: It is well known that watershed segmentation works through the analysis of topographic morphology, which is difficult to perform directly on the original 3-D LiDAR point cloud due to nonuniformly distributed and unstructured characteristics. Therefore, prior to the marker-controlled watershed segmentation-based coarse segmentation, a rasterized CHM is first required and generated. The CHM is a 2-D surface model that expresses the height of the upper canopy surface above the ground. Indeed, it eliminates the effect of topographic relief on the tree canopy height, thus reflecting the height fluctuation of the forest canopy, and also plays a significant role in the inversion of forest parameters or forest biomass. In our implementation, the elevation value of each point in the DSM is subtracted from the corresponding ground elevation value, and the normalized point cloud is obtained. Then, the CHM is derived from the normalized point cloud through interpolation techniques. Since the noises contained in the generated CHM may affect the determination of local maxima, a fixed window size Gaussian filter (in this article, the template size is set  $5 \times 5$ , sigma is set 0.5) is used to smooth the CHM for alleviating the noises. As a result, the Gaussian canopy height model (GCHM) is produced, as shown in Fig. 2.

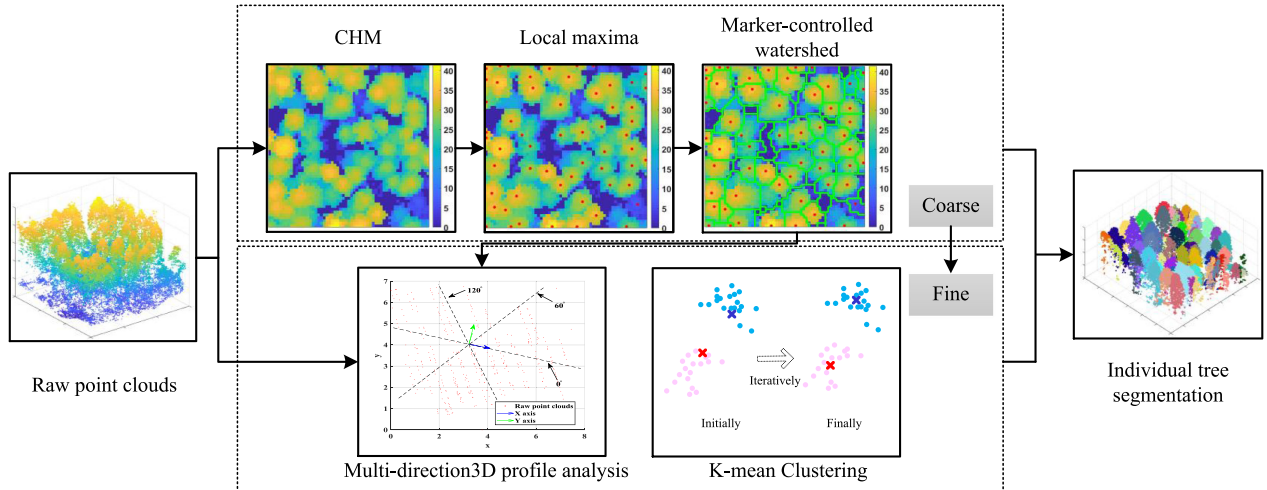


Fig. 1. Workflow of the proposed method.

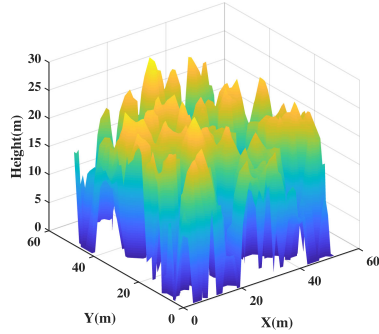


Fig. 2. 3-D display of individual trees within a local GCHM. The GCHM is rendered from blue to yellow according to height values.

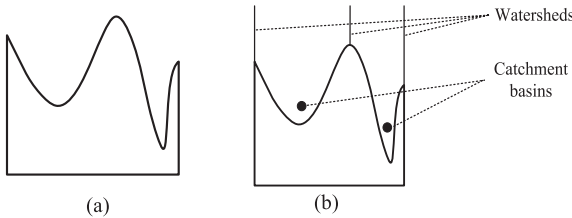


Fig. 3. Illustration of the concept of watershed segmentation. (a) Profile of gray-level image. (b) Catchment basins and watersheds.

**2) Coarse Segmentation From a Marker-Controlled Watershed Segmentation:** After the GCHM generation, a marker-controlled watershed segmentation is carried out for coarse segmentation. Watershed segmentation is a powerful image segmentation method that has its basis in mathematical morphology [43]. It considers a gray-level image as topographic surface, where the gray value of each pixel is interpreted as altitude. Fig. 3 shows the concept of watershed segmentation, and its efficient implementation may be obtained based on immersion simulations [44]. More specifically, suppose a water source is placed in each regional minimum and the entire topography structure is flooded from below. When water from

two sources (i.e., regional minima) are about to meet, a dam is constructed to prevent the merging. The flooding and dam construction process continues until only the dams are visible from above. Consequently, these dams, i.e., the watershed lines, effectively segment the image into a set of regions, i.e., catchment basins.

It is worthy to notice that if a watershed segmentation algorithm is performed using all local minima within the GCHM image, all the contours between two minima will be present and then an over-segmented image will occur. Apparently, there are several possible solutions to this problem. One of them is to start the watershed from selected points only. In this case, only the contours dividing marked regions are detected. Therefore, a unique marker has to be found. Unlike the watershed segmentation algorithm, the marker-controlled watershed segmentation algorithm alleviates the over-segmentation through the input of “markers” that correspond to the positions of objects to be segmented. In this case, the selection of “markers” affects the performance of the segmentation. As shown in Fig. 2, we can summarize that single tree point clouds acquired from airborne LiDAR usually exhibit the following characteristics: (1) the elevation of a tree apex is higher than that of the rest of the tree crown; (2) the maximum elevation of a single tree crown is the top of the tree. Based on these assumptions, we performed local maximum filtering for determining the positions of individual tree apexes as markers in the marker-controlled watershed algorithm. In our implementation, we define a local sliding window with a fixed size (set  $7 \times 7$  in this article) to find the positions of individual tree apexes. In Fig. 4(a), the identified individual tree apexes are marked in red.

Afterward, the GCHM image is reversed and further modified based on minima imposition technique [45], which makes regional minima occur at marker pixels. Finally, the marker-controlled watershed segmentation algorithm is performed on the modified GCHM image for producing a set of coarsely segmented individual trees. Some typical watershed segmentation results are demonstrated in Fig. 4(b) and the tree crowns are highlighted in GREEN polygons. Consequently, these polygons

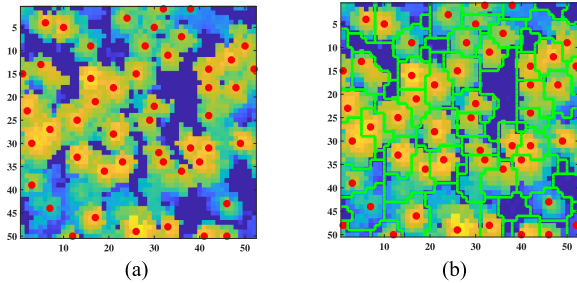


Fig. 4. Example of marker-controlled watershed segmentation. The GCHM is rendered according to the values of height from blue to yellow. The identified individual tree apexes are marked in red and the tree crowns are highlighted in green polygons. (a) Tree apex positions derived local maximum methods. (b) Crown delineation display.

are used as references to assign each point in the normalized LiDAR point clouds into the corresponding point cluster for achieving the coarse individual tree segmentation.

#### A. Three-Dimensional Point Cloud-Based Fine Segmentation

After the coarse segmentation, the 3-D point cloud-based fine segmentation is carried out on each point cluster. As a matter of fact, the sliding window size selection places a severe constraint on the performance of the local maximum filter, thus affecting the coarse segmentation results derived from the marker-controlled watershed segmentation. That is, if the sliding window is small for the local maximum detection methods, more local maxima can be identified, but the larger crowns will be divided into multiple vegetation. Otherwise, the number of local maxima identified is small, and many smaller crowns are merged into one crown. As shown in Fig. 5, the tree apex positions obtained using the local maximum detection method based on the fixed sliding window size are used as markers of the marker-controlled watershed algorithm to produce the error segmentation result. To date, some studies have also been developed in an attempt to address this issue. Empirically, the crown width of one tree is related to its height and their relationship is inverted for establishing a variable sliding window size to enhance the detection performance of tree apex. Although the local maxima detection method using the variable-size sliding window improves the detection efficiency of individual tree apex positions [46], its performance is largely limited by the established empirical regression model between crown width and tree height. To address the limitations from which the existing methods suffer, the 3-D point cloud-based fine segmentation through the combination of a multidirectional 3-D profile analysis and K-means clustering [28] is carried out on each point cluster after the coarse segmentation. As shown in Fig. 6, the key insight behind the fine segmentation is that the peaks of the shape fitting curve from the multidirectional 3-D profiles are considered as the potential tree apexes, hence, the calculated potential tree apexes are used as the traditional K-means clustering algorithm prior for iteratively producing a robust segmentation.

1) *Spatial Profiles for Robustly Locating the Potential Tree Apexes:* The traditional K-means clustering algorithm is an unsupervised algorithm. Thus, given a point set, groups of

clusters are generated based on the Euclidean distance, i.e., by achieving the objective that allows short intracluster distances and large intercluster distances. However, the performance of traditional K-means clustering algorithm largely depends on the location and number of initial clustering centers, meaning a wrong initial allocation often leads to a suboptimal solution. For the task of single tree segmentation, the number of seeds for K-means clustering algorithm is directly related to those of the individual trees within the current cluster. Thus, the number of possible individual trees can be used as a prior to improve the performance of the traditional K-means clustering algorithm.

In field surveys, the location of an individual tree is correctly measured at the bottom of its stem. Unfortunately, the point density of airborne LiDAR point clouds usually decreases from top to bottom, which results in the fact that the amount of tree trunk/stem structure details is relatively less compared with the rest of the tree crown. As a result, it is difficult for airborne LiDAR point clouds to accurately locate the positions of individual tree stems due to the lack of understory information [37], especially in overlapped forests. Similar to tree stems, the tree apexes are also used as markers of individual trees, which represents the specific number of individual trees in point clouds to be processed. Therefore, the spatial profile analysis is proposed for robustly locating the potential tree apexes.

Fig. 7 shows the concept of the 3-D profile analysis in a certain direction. Fig. 7(a) shows the location of the current profile in 3-D space. Then, 3-D profile points on the current profile are extracted from the current point cluster in a certain direction [as shown in Fig. 7(b)] and the local maximum points are chosen using an established local maximum histogram [as shown in Fig. 7(c)]. Afterward, the shape curve corresponding to the local maximum point is fitted by a cubic polynomial interpolation method [as shown in Fig. 7(d)], and then the peak value of the fitting curve is calculated as the potential tree apex [as shown in Fig. 7(d)]. By doing this, the potential tree apexes on the current profiles can be robustly located.

2) *Local Coordinate Reference Establishment for Multidirectional Spatial Profile Analysis:* As mentioned earlier, we attempt to refine the coarse individual tree segmentation results in Section III-A through the multidirectional 3-D spatial distribution analysis. The detailed description of the 3-D profile analysis in a certain direction is given in Section III-B1. However, for the multidirectional 3-D profile analysis, its performance and robustness depend on the location selection and combination of profiles. Consequently, to investigate how the potential tree apexes are easily on the profiles, the spatial distributions of the point clusters are analyzed. Fig. 8 shows fitting results of the projection contours of individual and multiple trees. Generally, the projection contour and spatial distribution of single tree point clouds in the horizontal plane is approximately circular, while that of multiple tree point clouds is approximately elliptical [36]. It is obvious that the tree apexes of multiple trees are more likely to appear along the major axis of the projected ellipse. That is to say, the tree apex of multiple trees can be detected more easily if we section the point cluster along the major axis of its projected ellipse.

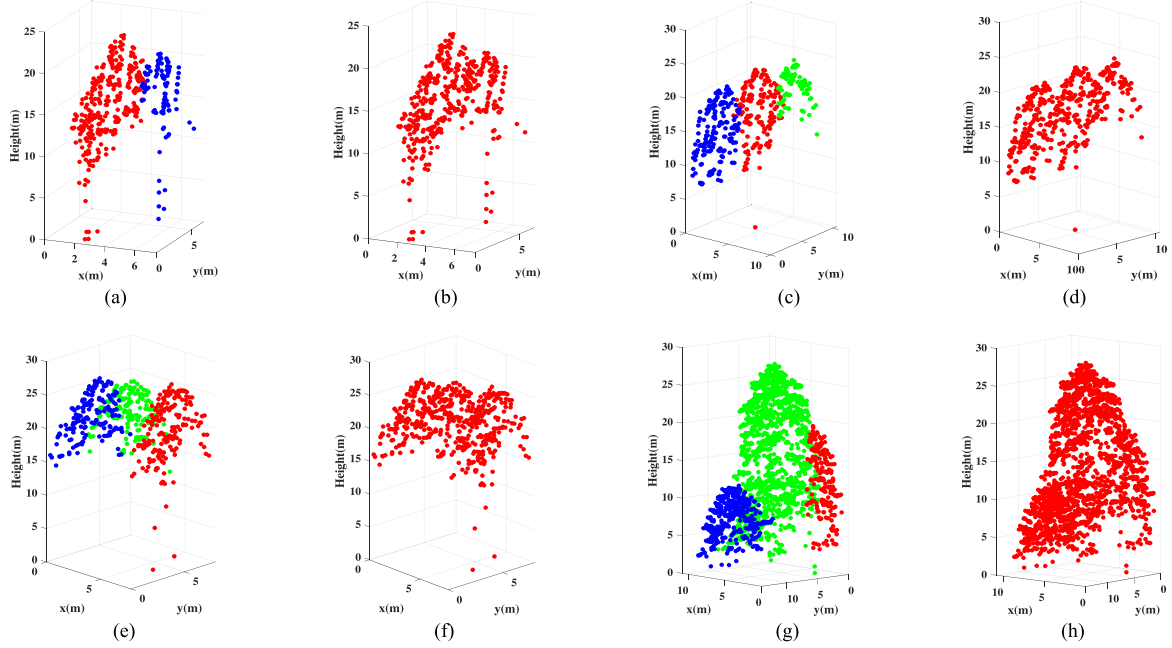


Fig. 5. Wrong examples of coarse segmentation. Individual trees are colored in different colors. (a) Ground Truth (Example. #1). (b) Coarse segmentation (Example #1). (c) Ground Truth (Example #2). (d) Coarse segmentation (Example #2). (e) Ground Truth (Example #3). (f) Coarse segmentation (Example #3). (g) Ground Truth (Example #4). (h) Coarse segmentation (Example #4).

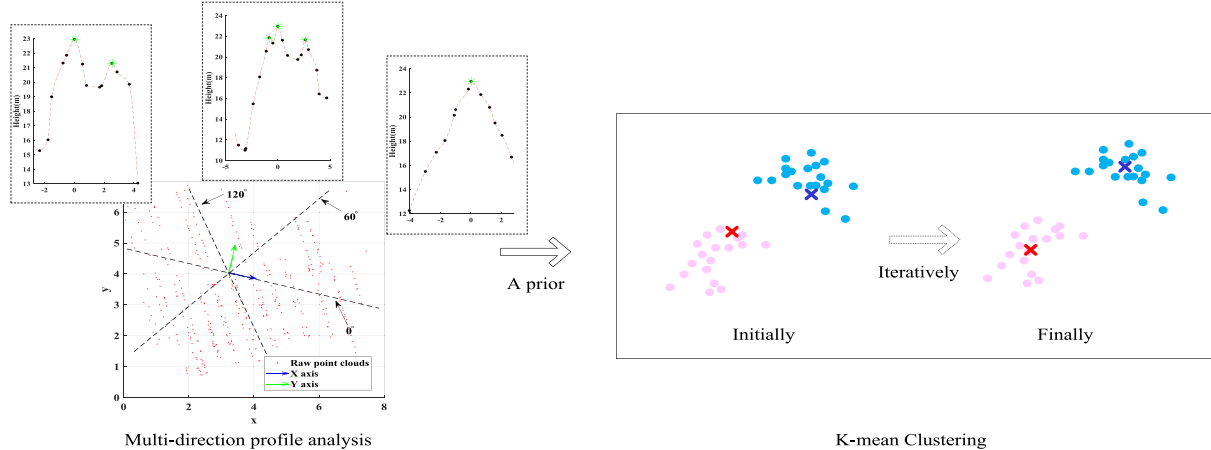


Fig. 6. Key insight behind the fine segmentation of combining the multidirectional profile analysis and K-means clustering. For multidirectional profile analysis, the red solid circles are the projected points from the extracted LiDAR points on the current profile, black solid circles are LiDAR points on the current profile, green stars are the local maxima, and red dot lines are the fitted shape curve. For K-means clustering, different colors represent different clusters and their associated cluster centers.

Hence, we first establish a local coordinate reference framework before performing the multidirectional 3-D spatial distribution analysis, which will provide guidance for the profile location selection.

More specifically, prior to the multidirectional 3-D profile analysis, we construct a local coordinate reference framework for each point cluster, the  $x$ -axis of which needs to be aligned with the major axis of the projected ellipse. Since the spatial distribution of the point clusters is analyzed in 2-D space, we first project the raw 3-D point clouds into the  $xyz$  plane. Then, we perform a PCA on the 2-D projected point cluster to

establish a local coordinate reference framework for providing the guidance of the profile selection at the subsequent procedure. In our implementation, we construct a local coordinate reference system at each point cluster from Section III-A2 by conducting an eigenvalue decomposition on the 2-D covariance matrix  $C_p^{2d}$ . The details of establishment are as follows: The raw 3-D point cluster is projected onto the  $xoy$  plane and the 2-D covariance matrix  $C_p^{2d}$  is constructed as defined in the following:

$$C_p^{2d} = \frac{1}{|N|} \sum_{i=1}^n (p_i^{2d} - \bar{p}^{2d}) (p_i^{2d} - \bar{p}^{2d})^T \quad (1)$$

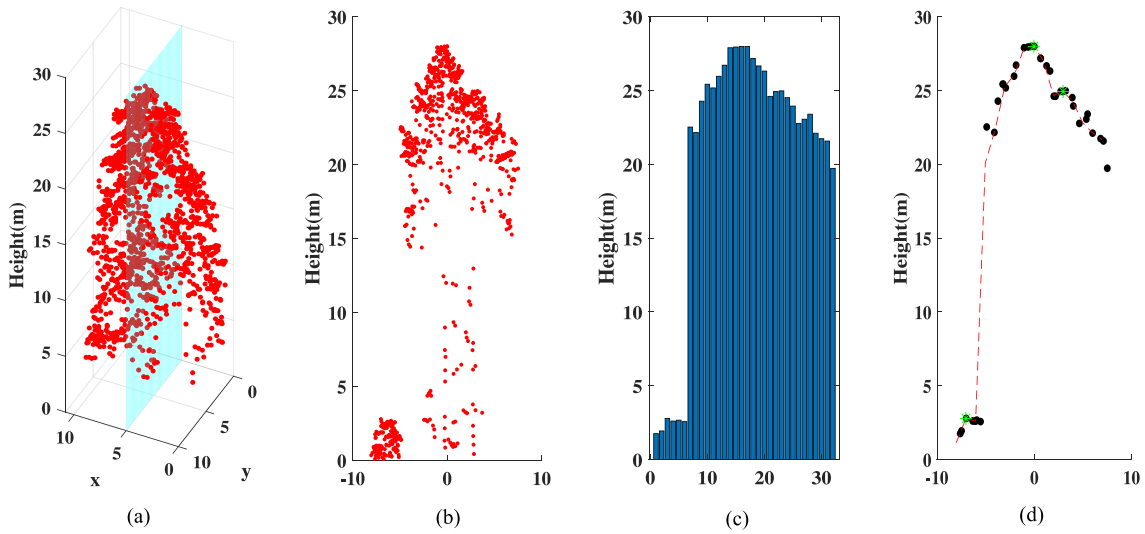


Fig. 7. Concept of the profile analysis. In (a), the red solid circles are the extracted LiDAR points in 3-D space and the light blue plane is the current profile. In (b), the red solid circles are the extracted LiDAR points on the current profile. The value of each bin in (c) is the local maximum height. In (d), black solid circles are LiDAR points on the current profile, green stars are the local maxima, and red dot lines are the fitted shape curve.

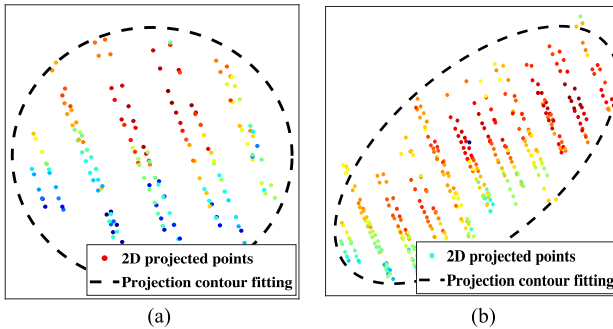


Fig. 8. Fitting results of projection contours of individual and multiple trees. The 2-D projected points are rendered according to their heights from blue to red. (a) Individual tree. (b) Multiple trees.

where  $\bar{p}^{2d} = \frac{1}{|N|} \sum_{i=1}^n p_i^{2d}$  and  $n$  denotes the number of points within the current point cluster. Following this, the 2-D covariance matrix  $C_p^{2d}$  is decomposed in order to establish the local coordinate reference framework, where the eigenvector corresponding to the maximum eigenvalue is the  $x$ -axis, the eigenvector corresponding to the minimum eigenvalue is the  $y$ -axis, the  $z$ -axis is perpendicular to the  $xyz$  plane, and the origin is the tree apex detected by the local maximum filter in Section III-A2. Fig. 9(a) shows the established local coordinate reference framework in 3-D space.

*3) Combining Multidirectional Profile Analysis and K-Means Clustering for Fine Segmentation:* After the local coordinate reference framework of the current point cluster is constructed in Section III-B2, the projected 2-D point clusters are remapped into 3-D space. That is, the fine segmentation, which combines multidirectional profile analysis and K-means clustering is conducted in the 3-D space. The multidirectional 3-D spatial distribution analysis starts with profile generation, which sections the point cluster from  $0^\circ$  to  $180^\circ$  in increments

of specific direction interval into a set of profiles for further analysis. Fig. 9 is an example of local maximum shape curve fitting of multidirectional 3-D spatial profiles when the direction interval is set to  $60^\circ$ , which means that we will section each point cluster in the  $0^\circ$ ,  $60^\circ$ , and  $120^\circ$  directions in our implementation. Fig. 9(b) shows the locations of profiles from the top view and Fig. 9(c) and (d) shows the corresponding fitting shape curves, respectively.

The potential tree apex position obtained from the multidirectional 3-D profile analysis is then judged based on neighborhood relation and a height difference rule to eliminate the detected pseudo tree apex [47], and the refined potential tree apex is used as the initial clustering center of K-means clustering algorithm. Finally, the height of the current point cluster is scaled down [48] and iterative K-means clustering is performed to refine the 3-D segmentation for generating the individual trees.

#### IV. EXPERIMENTATION AND ANALYSIS

In this section, a brief description about the experimental data and evaluation criteria is first given. Then, we qualitatively and quantitatively analyze the performance of the results derived from the proposed method, respectively.

##### A. Experimental Data and Evaluation Criteria

To verify the effectiveness and robustness of the proposed method, experiments are performed on the public NEWFOR dataset for the qualitative and quantitative analysis. The public NEWFOR dataset [16] aims to improve and promote the application of new remote sensing technologies, such as LiDAR, in forest resources investigation and management so as to better understand and improve forest management strategies. The study area covered by the dataset includes different forest types, forest structure, point density etc.. The data in each study

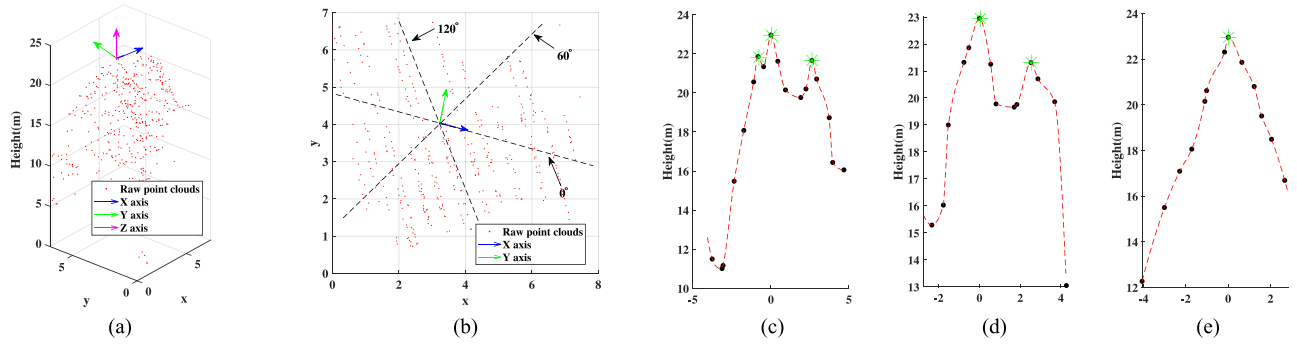


Fig. 9. Example for local maximum shape curve fitting of multidirectional 3-D spatial profiles when the direction interval is set to 60°. Red points in (a) are LiDAR points. In (b)–(d), black solid circles are LiDAR points on current profile, green stars are the local maxima, and red dot lines are the fitted shape curve. (a) 3-D display and local coordinate system. (b) 2-D top view for displaying the location of profiles. (c) 0° profile. (d) 60° profile. (e) 120° profile.

TABLE I  
DETAILED INFORMATION OF SAMPLE PLOT

Plot #	Study area	Country/region	Location	Density/(m <sup>2</sup> )	Forest type	Minimum height(m)	Maximum height(m)
1	Cotolivier	Italy	45°2' N 6°46' E	11	Coniferous forest (Scots pine and larch)	2.736	26.213
2	Leskova	Slovenia	45°39' N 14°28' E	30	Mixed forest (Fir, spruce, and beech)	6.1	39.6

area include LiDAR point clouds collected by different sensors, digital terrain model with a spatial resolution of 0.5 m × 0.5 m or 1.0 m × 1.0 m, and field position, height and diameter at breast height of individual trees. Table I summarizes the related information of sample plots used in this article. Both sample plots are single layered forests, where plot #1 is coniferous forest and plot #2 is mixed forest. Parameters, such as stem locations, tree heights, and information about species composition are provided.

The performance evaluation of the proposed method is a key issue in the whole modeling process. This article evaluates the individual tree segmentation results from two aspects. The first is to calculate the correlation coefficient  $R^2$  and root mean square error (RMSE) between the field height and positions, and the estimated results derived from LiDAR point clouds, as defined in (2) and (3). In general, the larger the value of  $R^2$ , the better the estimation. The smaller the RMSE value, the better the estimation. Second, after automatic matching with field data [40], the segmentation results are quantitatively evaluated by four evaluation criteria [extraction rate (ER), match rate (MR), commission rate (CR), and omission rate (OR)], as defined in (4)–(7)

$$R^2 = 1 - \frac{\sum_{i=1}^n (y_i - \hat{y}_i)^2}{\sum_{i=1}^n (y_i - \bar{y}_i)^2} \quad (2)$$

$$\text{RMSE} = \sqrt{\frac{\sum_{i=1}^n (y_i - \hat{y}_i)^2}{n-1}} \quad (3)$$

where  $y_i$  denotes the field value,  $\hat{y}_i$  denotes the estimated value,  $\bar{y}_i$  denotes the mean value, and  $n$  denotes the number of samples

$$\text{ER} = \frac{N_{\text{test}}}{N_{\text{ref}}} \times 100\% \quad (4)$$

$$\text{MR} = \frac{N_{\text{match}}}{N_{\text{ref}}} \times 100\% \quad (5)$$

$$\text{CR} = \frac{N_{\text{com}}}{N_{\text{test}}} \times 100\% \quad (6)$$

$$\text{OR} = \frac{N_{\text{om}}}{N_{\text{ref}}} \times 100\% \quad (7)$$

where  $N_{\text{test}}$  is the number of trees from the proposed method,  $N_{\text{ref}}$  is the number of field trees,  $N_{\text{match}}$  is the number of the correctly matched trees,  $N_{\text{com}}$  is the number of incorrectly matched trees among the trees from the proposed method, and  $N_{\text{om}}$  is the number of incorrectly matched trees among field trees.

### B. Qualitative Evaluation

For qualitative evaluation, this section illustrates the visual comparisons of segmentation results as aforementioned. Fig. 10 shows two comparison examples before and after segmentation refinement. The results before segmentation refinement is only from the marker-controlled watershed segmentation algorithm. More specifically, after the 2-D contour of single tree crowns are extracted from the rasterized CHM using the marker-controlled watershed algorithm, each single tree polygon segment on CHM is considered a reference. These references are used to select the

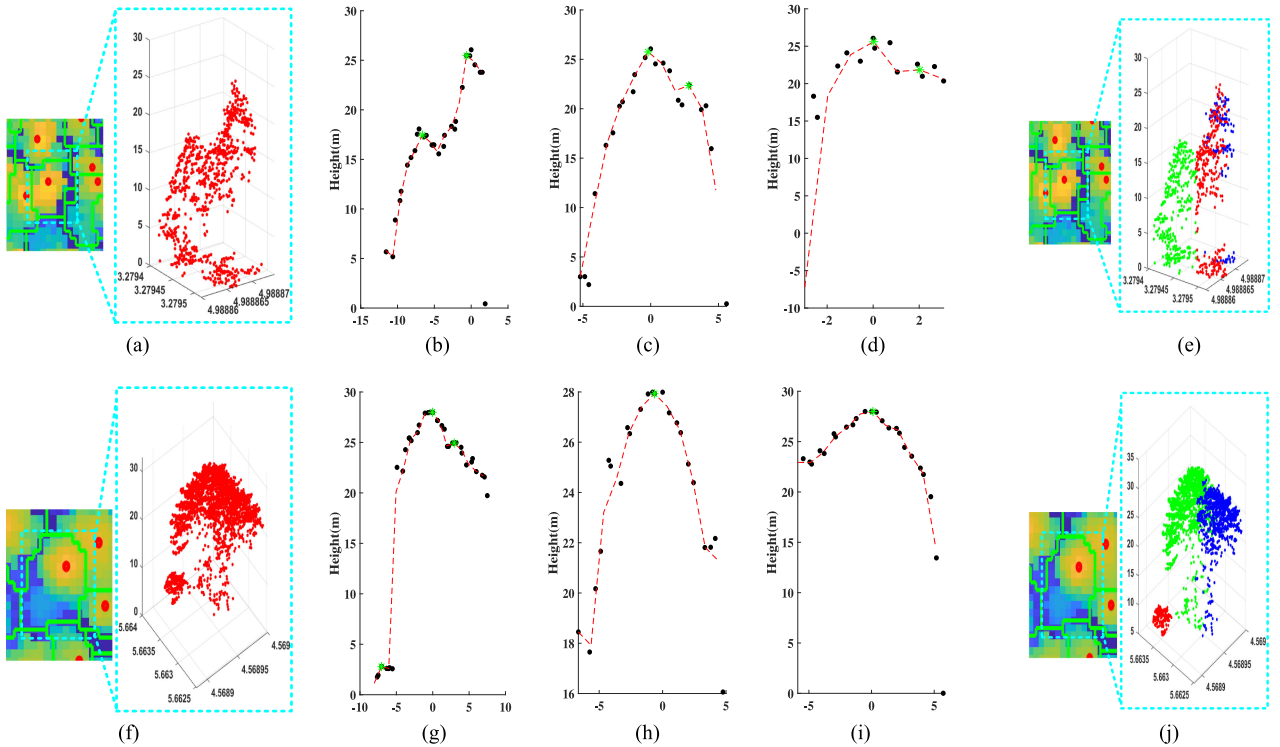


Fig. 10. Comparisons between with and without optimization. In (a), (e), (f), and (j), different extracted individual trees are rendered using red, green, and blue. In (b)–(d) and (g)–(i), black solid circles are LiDAR points on current profile, green stars are the local maxima corresponding the refined tree apexes, and red dot lines are the fitted shape curve. (a) Before segmentation refinement (example #1). (b)  $0^\circ$  profile (example #1). (c)  $60^\circ$  profile (example #1). (d)  $120^\circ$  profile (example #1). (e) After segmentation refinement (example #1). (f) Before segmentation refinement (example #2). (g)  $0^\circ$  profile (example #2). (h)  $60^\circ$  profile (example #2). (i)  $120^\circ$  profile (example #2). (j) After segmentation refinement (example #2).

points belonging to the 2-D contour of the CHM in the normalized LiDAR point clouds for achieving the coarse individual tree segmentation. In Fig. 10(a) and (f), the tree group consisting of individual trees with different heights was segmented together by the marker-controlled watershed segmentation algorithm.

For each point cluster corresponding to the segmented individual tree, the local coordinate reference framework is established through covariance matrix decomposition. Following this, the potential tree apexes are obtained by profiling the current point cluster in the following three directions, i.e.,  $0^\circ$ ,  $60^\circ$ , and  $120^\circ$ , which can be used as a prior of K-means clustering algorithm to complete single tree detection. As shown in Fig. 10(b)–(d) and (g)–(i), the multidirectional profile analysis is performed to detect the tree apexes of each point cluster, where green stars are the local maxima corresponding to the refined tree apexes. Hence, it can be concluded that through the multidirectional profile analysis of 3-D point cloud, the adjacent potential tree apex can be effectively identified, and the accuracy of single tree detection can be improved. As shown in Fig. 10(e) and (j), the tree group consisting of individual trees is segmented into multiple trees by using the K-means clustering algorithm with a prior, where different extracted individual trees are rendered using red, green, and blue. Fig. 11(a) and (b) show the overview of 3-D segmentation results over two sample plots, in which different individual trees are colored in different colors. Fig. 12 shows some of the individual trees, which suggests that the

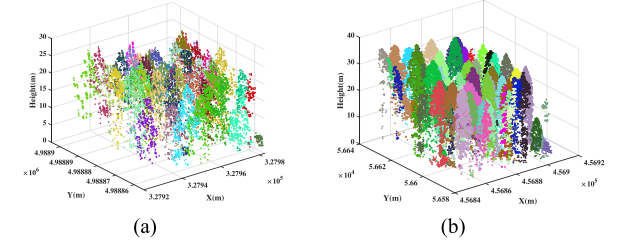


Fig. 11. 3-D display of segmentation results. Different individual trees are rendered using random colors. (a) Sample plot #1. (b) Sample plot #2.

proposed method can effectively extract the complete structure of individual trees.

### C. Quantitative Evaluation

*1) Role of Multidirectional Profile Analysis in Segmentation Results:* The tree apex is a crucial indicator, which suggests the positions of individual trees. Thus, the tree apexes are always used as a prior for assisting the implementation of the marker-controlled watershed segmentation algorithm. As mentioned in Section III-B, the potential tree apexes remarkably affect the segmentation results. Consequently, the multidirectional profile analysis is presented in this article to enhance the segmentation performance. To investigate the role of multidirectional profile analysis in the segmentation results, the results derived from

TABLE II  
ROLE OF MULTIDIRECTIONAL PROFILE ANALYSIS IN SEGMENTATION RESULTS

Methods	Extraction Rate (%)	Match Rate (%)	Commission rate (%)	Omission rate (%)
Marker-controlled watershed segmentation	93.1	59.8	35.7	40.2
<b>Proposed method</b>	<b>107.8</b>	<b>67.6</b>	<b>37.3</b>	<b>32.5</b>

The performance from the proposed method is highlighted in BOLD fonts.

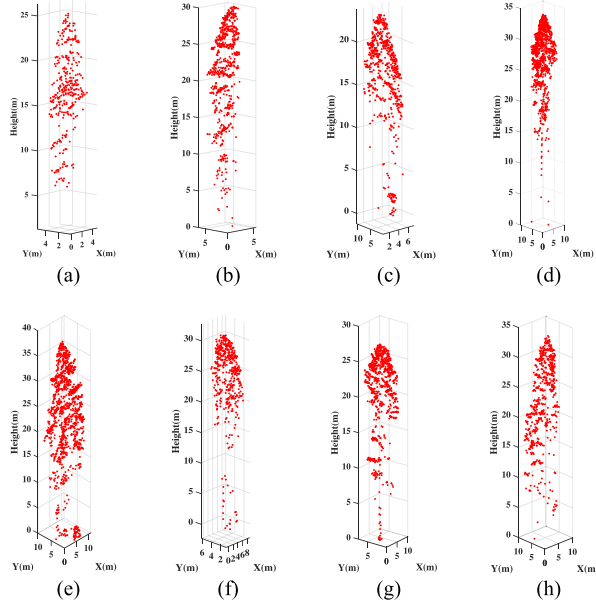


Fig. 12. Three-dimensional visualization of extracted individual trees. Red points are individual trees. (a) Example #1. (b) Example #2. (c) Example #3. (d) Example #4. (e) Example #5. (f) Example #6. (g) Example #7. (h) Example #8.

both the conventional marker-controlled watershed segmentation algorithm and the proposed method are compared in this section. Table II outlines the comparison results, where the results from the proposed method is highlighted in bold fonts. Results demonstrated that the proposed method is superior to the conventional marker-controlled watershed segmentation algorithm, with differences of approximately 14.7% in extraction rate and approximately 7.8% in match rate. Furthermore, the omission rate is reduced from 40.2% to 32.5%. In summary, the multidirectional profile analysis is efficient to optimize the detection of the tree apexes for further improving the segmentation of individual trees.

**2) Effect of Profile Direction Interval on Segmentation Results:** As mentioned earlier, both multidirectional profile analysis and K-means clustering algorithm are integrated together to robustly segment individual trees, which remarkably enhances the segmentation performance. Moreover, the direction interval in multidirectional profile analysis determines the detection performance of the proposed method to some extent. In order to verify the effect of the profile direction interval on segmentation results, experiments are conducted using sample plot #1, where the direction interval is set to 30°, 45°, 60°, and 90°, respectively. Fig. 13 illustrates the fluctuation in extraction rate, matching rate, commission rate,

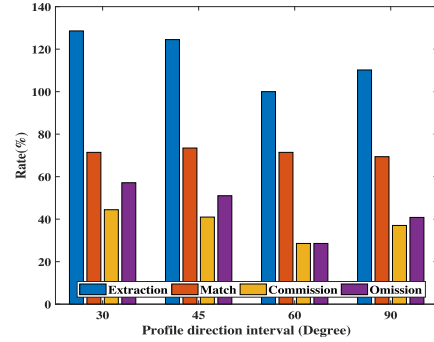


Fig. 13. Effect of profile direction interval on segmentation results (Plot #1).

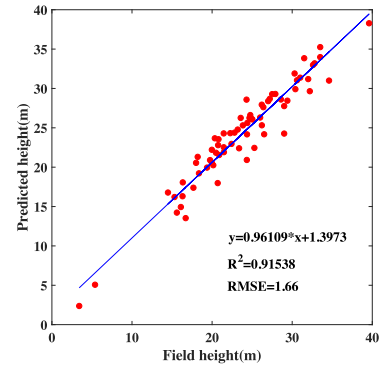


Fig. 14. Scatter plots of extracted tree height and reference tree height.

and omission rate of segmentation results for different profile direction intervals. The experimental results indicate that, when the profile direction interval is equal to 60°, the matching rate can be higher with a lower commission rate and omission rate. Smaller profile direction interval results in a larger extraction rate, and correspondingly a larger commission rate. Moreover, the profile analysis in this article is based on the established local coordinate framework, which reduces the possibility of tree apexes along the y-axis of the local coordinate framework. Consequently, when the direction interval of the profile equals 90°, higher commission rate and omission rate occur.

**3) Analysis of Tree Height Estimation:** To verify the correctness of the estimated height derived from the proposed method, the proposed method is used to detect the positions of individual trees (in which the profile direction interval is set to 60°). This is also one way of demonstrating the accuracy of the estimated height. The information of the tree top height is obtained and compared with the field tree height. The comparison results of the field tree heights and the estimated ones are shown in Fig. 14. The x-axis represents the field value of tree heights and the

TABLE III  
COMPARISONS AMONG DIFFERENT METHODS

Methods	Extraction Rate (%)	Match Rate (%)	Commission rate (%)	Omission rate (%)	RMSE <sub>Vertical</sub> (m)	RMSE <sub>Horizontal</sub> (m)
Local maxima + Filtering	51.0	45.0	9	59	1.60	0.90
Local maxima + Region growing	57.0	43.0	20	61	1.80	1.20
Local maxima + Multiscale CHM	101.0	46.0	61	57	1.70	0.70
Segmentation + Clustering	139.0	53.0	95	51	1.70	1.00
Mean shift segmentation	115.2	65.1	31.3	35.9	1.59	0.80
Horizon slice + vertical merging	99.3	59.0	45.4	49.1	1.70	0.92
<b>Proposed method</b>	<b>107.8</b>	<b>67.6</b>	<b>37.3</b>	<b>32.5</b>	<b>1.66</b>	<b>0.89</b>

The performance of the proposed method is highlighted in BOLD fonts and the best performance is highlighted in RED fonts.

y-axis represents the ones estimated from the proposed method. Although there are some errors between the field value and the ones estimated, the field value and the estimated value of tree heights satisfy a good linear relationship. The correlation coefficient  $R^2 = 0.91$  and root mean square error RMSE = 1.66 between the field value and the estimated value show that the proposed method can better estimate the individual tree heights.

4) *Comparison With Other Existing Methods:* In order to further evaluate the effectiveness of the proposed method, it is quantitatively compared with other existing methods, including local maxima + multiscale CHM [16], segmentation + clustering [16], local maxima + filtering [49], local maxima + region growing [50], mean shift segmentation [38], and horizon slice + vertical merging [34]. The experimental results derived from these methods (i.e., local maxima + multiscale CHM [16], segmentation + clustering [16], local maxima + filtering [49], local maxima + region growing [50]) were available in literature [16] for objective comparisons, mean shift segmentation [38], and horizon slice + vertical merging [34] are state-of-art methods. Mean shift segmentation method considers the tree group as a multimodal distribution, which assumes the highest point density is usually the top of the tree. Horizon slice + vertical merging method performs K-means clustering on the horizon slices and then merges the clusters in the vertical direction. Table III summarizes the differences in extraction rate, match rate, commission rate, omission rate, vertical RMSE, and horizontal RMSE of tree heights among the different methods. The experimental results show that the match rate of the proposed method is obviously better than that of other existing methods, with an average difference of more than 15%. Compared with other existing methods, the proposed method achieves a lower omission rate, which is more than 6.3% lower on average. Although the proposed method presents a relatively higher commission rate than both local maxima + filtering and local maxima + region growing, it has a higher extraction rate and a lower commission rate. Additionally, the proposed method is superior to mean shift segmentation, with difference in match rate and omission rate. When it comes to the vertical RMSE of tree heights, the proposed method is superior to local maxima + region growing, local maxima + multiscale CHM, segmentation + clustering, and horizon slice + vertical merging. Although the proposed method is slightly higher than local maxima + filtering in the vertical RMSE, the proposed method

has higher extraction rate, match rate, and lower omission rate than local maxima + filtering. In terms of the horizontal RMSE, the proposed method has the same precision as local maxima + filtering, which is significantly lower than both local maxima + region growing and segmentation + clustering. Although our horizontal RMSE is higher than local maxima + multiscale CHM, the proposed method has obvious advantages in match rate, commission rate, and omission rate.

## V. CONCLUSION

Due to the increasing demand of airborne LiDAR for forest planning and management, single-tree detection based on airborne LiDAR has become a hot topic. To address the problem where the performance of CHM-based methods is limited by the search window size, this article develops an individual tree segmentation method based on the marker-controlled watershed algorithm and a 3-D spatial distribution recognition from airborne LiDAR point clouds. First, based on the coarse segmentation derived from CHM, the idea of point cloud distribution recognition in 3-D space is introduced for carrying out the multidirectional spatial distribution analysis to refine the potential tree apex positions, which effectively improves the efficiency of tree apex detection. Second, taking the spatial distribution pattern of the tree group into consideration, the PCA-based method is used to establish the local coordinate system, which guides the location selection of 3-D spatial profiles. Finally, the refined potential tree apex positions are used as a prior of K-means clustering algorithm to realize the 3-D coarse-to-fine segmentation of single trees. Although the proposed method can improve the detection accuracy of tree apex positions by analyzing the horizontal profile structure in 3-D space, it fails on multilayer forest structure. In the future, the vertical profile structure analysis will be one of our focus. Meanwhile, on the basis of single tree detection, our next step will be to analyze and extract the 3-D structural parameters of single tree crowns, and to study the actual crown structure and its dynamic changes at stand level.

## REFERENCES

- [1] S. W. Running and J. C. Coughlan, "A general model of forest ecosystem processes for regional applications I. Hydrologic balance, canopy gas exchange and primary production processes," *Ecological Modelling*, vol. 42, no. 2, pp. 125–154, 1988.

- [2] A. Frick and S. Tervooren, "A framework for the long-term monitoring of urban green volume based on multi-temporal and multi-sensoral remote sensing data," *J. Geovisualization Spatial Anal.*, vol. 3, no. 1, 2019, Art. no. 6.
- [3] J. A. Turner, J. Buongiorno, and S. Zhu, "An economic model of international wood supply, forest stock and forest area change," *Scand. J. Forest Res.*, vol. 21, no. 1, pp. 73–86, 2006.
- [4] I. Indirabai, M. H. Nair, J. R. Nair, and R. R. Nidamanuri, "Estimation of forest structural attributes using ICESat/GLAS-spaceborne laser altimetry data in the western ghats region of India," *J. Geovisualization Spatial Anal.*, vol. 3, no. 2, 2019, Art. no. 10.
- [5] A. Suratno, C. Seielstad, and L. Queen, "Tree species identification in mixed coniferous forest using airborne laser scanning," *ISPRS J. Photogrammetry Remote Sens.*, vol. 64, no. 6, pp. 683–693, 2009.
- [6] Y. Sun, Q. Xin, J. Huang, B. Huang, and H. Zhang, "Characterizing tree species of a tropical wetland in southern China at the individual tree level based on convolutional neural network," *IEEE J. Sel. Topics Appl. Earth Observ. Remote Sens.*, vol. 12, no. 11, pp. 4415–4425, Nov. 2019.
- [7] S. A. Knowe, G. R. Ahrens, and D. S. DeBell, "Comparison of diameter-distribution-prediction, stand-table-projection, and individual-tree-growth modeling approaches for young red alder plantations," *Forest Ecology Manage.*, vol. 98, no. 1, pp. 49–60, 1997.
- [8] G. J. Newnham *et al.*, "Terrestrial laser scanning for plot-scale forest measurement," *Current Forestry Rep.*, vol. 1, no. 4, pp. 239–251, 2015.
- [9] L. K. Dorren, B. Maier, and A. Seijmonsbergen, "Improved Landsat-based forest mapping in steep mountainous terrain using object-based classification," *Forest Ecology Manage.*, vol. 183, no. 1/3, pp. 31–46, 2003.
- [10] H.-E. Andersen, R. J. McGaughey, and S. E. Reutebuch, "Estimating forest canopy fuel parameters using LiDAR data," *Remote Sens. Environ.*, vol. 94, no. 4, pp. 441–449, 2005.
- [11] J. Fang, A. Chen, C. Peng, S. Zhao, and L. Ci, "Changes in forest biomass carbon storage in China between 1949 and 1998," *Science*, vol. 292, no. 5525, pp. 2320–2322, 2001.
- [12] R. Nelson, W. Krabill, and J. Tonelli, "Estimating forest biomass and volume using airborne laser data," *Remote Sens. Environ.*, vol. 24, no. 2, pp. 247–267, 1988.
- [13] P. R. Coppin and M. E. Bauer, "Digital change detection in forest ecosystems with remote sensing imagery," *Remote Sens. Rev.*, vol. 13, no. 3–4, pp. 207–234, 1996.
- [14] M. Schlerf and C. Atzberger, "Inversion of a forest reflectance model to estimate structural canopy variables from hyperspectral remote sensing data," *Remote Sens. Environ.*, vol. 100, no. 3, pp. 281–294, 2006.
- [15] Y. Lin, A. Jaakkola, J. Hyppä, and H. Kaartinen, "From TLS to VLS: Biomass estimation at individual tree level," *Remote Sens.*, vol. 2, no. 8, pp. 1864–1879, 2010.
- [16] L. Eysn *et al.*, "A benchmark of LiDAR-based single tree detection methods using heterogeneous forest data from the alpine space," *Forests*, vol. 6, no. 5, pp. 1721–1747, 2015.
- [17] B. Koch, U. Heyder, and H. Weinacker, "Detection of individual tree crowns in airborne LiDAR data," *Photogrammetric Eng. Remote Sens.*, vol. 72, no. 4, pp. 357–363, 2006.
- [18] Q. Chen, D. Baldocchi, P. Gong, and M. Kelly, "Isolating individual trees in a savanna woodland using small footprint LiDAR data," *Photogrammetric Eng. Remote Sens.*, vol. 72, no. 8, pp. 923–932, 2006.
- [19] D. Mongus and B. Žalík, "An efficient approach to 3D single tree-crown delineation in LiDAR data," *ISPRS J. Photogrammetry Remote Sens.*, vol. 108, pp. 219–233, 2015.
- [20] M. Parkan and D. Tuia, "Estimating uncertainty of point-cloud based single-tree segmentation with ensemble based filtering," *Remote Sens.*, vol. 10, no. 2, pp. 335–350, 2018.
- [21] T. Liu, J. Im, and L. Quackenbush, "A novel transferable individual tree crown delineation model based on fishing net dragging and boundary classification," *ISPRS J. Photogrammetry Remote Sens.*, vol. 110, pp. 34–47, 2015.
- [22] A. O. Ok and A. Ozdarici-Ok, "2-D delineation of individual citrus trees from UAV-based dense photogrammetric surface models," *Int. J. Digit. Earth*, vol. 11, no. 6, pp. 583–608, 2018.
- [23] T. Dong, Q. Zhou, S. Gao, and Y. Shen, "Automatic detection of single trees in airborne laser scanning data through gradient orientation clustering," *Forests*, vol. 9, no. 6, pp. 291–309, 2018.
- [24] F. Pirotti, "Assessing a template matching approach for tree height and position extraction from LiDAR-derived canopy height models of *Pinus pinaster* stands," *Forests*, vol. 1, no. 4, pp. 194–208, 2010.
- [25] A. Zaforemska, W. Xiao, and R. Gaulton, "Individual tree detection from UAV LiDAR data in a mixed species woodland," *ISPRS Geospatial Week 2019*, vol. XLII-2/W13, pp. 657–663, 2019.
- [26] J. Holmgren and E. Lindberg, "Tree crown segmentation based on a tree crown density model derived from airborne laser scanning," *Remote Sens. Lett.*, vol. 10, no. 12, pp. 1143–1152, 2019.
- [27] D. Marinelli, C. Paris, and L. Bruzzone, "An approach to tree detection based on the fusion of multitemporal LiDAR data," *IEEE Geosci. Remote Sens. Lett.*, vol. 16, no. 11, pp. 1771–1775, Nov. 2019.
- [28] F. Morsdorf, E. Meier, B. Allgöwer, and D. Nüesch, "Clustering in airborne laser scanning raw data for segmentation of single trees," *Int. Archives Photogrammetry, Remote Sens. Spatial Inf. Sci.*, vol. 34, no. part 3, p. W13, 2003.
- [29] W. Li, Q. Guo, M. K. Jakubowski, and M. Kelly, "A new method for segmenting individual trees from the LiDAR point cloud," *Photogrammetric Eng. Remote Sens.*, vol. 78, no. 1, pp. 75–84, 2012.
- [30] W. Yao, J. Krull, P. Krzystek, and M. Heurich, "Sensitivity analysis of 3D individual tree detection from LiDAR point clouds of temperate forests," *Forests*, vol. 5, no. 6, pp. 1122–1142, 2014.
- [31] X. Lu, Q. Guo, W. Li, and J. Flanagan, "A bottom-up approach to segment individual deciduous trees using leaf-off LiDAR point cloud data," *ISPRS J. Photogrammetry Remote Sens.*, vol. 94, pp. 1–12, 2014.
- [32] Y. Wang, H. Weinacker, B. Koch, and K. Sterenczak, "LiDAR point cloud based fully automatic 3D single tree modelling in forest and evaluations of the procedure," *Int. Archives Photogrammetry, Remote Sens. Spatial Inf. Sci.*, vol. 37, no. B6B, pp. 45–51, 2008.
- [33] E. Ayrey *et al.*, "Layer stacking: A novel algorithm for individual forest tree segmentation from LiDAR point clouds," *Can. J. Remote Sens.*, vol. 43, no. 1, pp. 16–27, 2017.
- [34] K. Kandare, H. O. Ørka, J. C.-W. Chan, and M. Dalponte, "Effects of forest structure and airborne laser scanning point cloud density on 3D delineation of individual tree crowns," *Eur. J. Remote Sens.*, vol. 49, no. 1, pp. 337–359, 2016.
- [35] A. Ferraz *et al.*, "3-D mapping of a multi-layered Mediterranean forest using ALS data," *Remote Sens. Environ.*, vol. 121, pp. 210–223, 2012.
- [36] W. Dai, B. Yang, Z. Dong, and A. Shaker, "A new method for 3D individual tree extraction using multispectral airborne LiDAR point clouds," *ISPRS J. Photogrammetry Remote Sens.*, vol. 144, pp. 400–411, 2018.
- [37] W. Yan, H. Guan, L. Cao, Y. Yu, S. Gao, and J. Lu, "An automated hierarchical approach for three-dimensional segmentation of single trees using UAV LiDAR data," *Remote Sens.*, vol. 10, no. 12, 2018, Art. no. 1999.
- [38] W. Xiao, A. Zaforemska, M. Smigaj, Y. Wang, and R. Gaulton, "Mean shift segmentation assessment for individual forest tree delineation from airborne LiDAR data," *Remote Sens.*, vol. 11, no. 11, 2019, Art. no. 1263.
- [39] A. M. Ramiya, R. R. Nidamanuri, and R. Krishnan, "Individual tree detection from airborne laser scanning data based on supervoxels and local convexity," *Remote Sens. Appl.: Soc. Environment*, vol. 15, 2019, Art. no. 100242.
- [40] A. Harikumar, F. Bovolo, and L. Bruzzone, "A local projection-based approach to individual tree detection and 3-D crown delineation in multi-storyed coniferous forests using high-density airborne LiDAR data," *IEEE Trans. Geosci. Remote Sens.*, vol. 57, no. 2, pp. 1168–1182, Feb. 2019.
- [41] L. Vincent and P. Soille, "Watersheds in digital spaces: An efficient algorithm based on immersion simulations," *IEEE Trans. Pattern Anal. Mach. Intell.*, vol. 13, no. 6, pp. 583–598, Jun. 1991.
- [42] S. Beucher, "Use of watersheds in contour detection," in *Proc. Int. Workshop Image Process., 1979: CCETT*, 1979, pp. 2.1–2.12.
- [43] S. Beucher and F. Meyer, "The morphological approach to segmentation: The watershed transformation," *Math. Morphology Image process.*, vol. 34, pp. 433–481, 1993.
- [44] P. Soille, *Morphological Image Analysis: Principles and Applications*. Berlin, Germany: Springer, 2013.
- [45] L. Vincent, "Morphological grayscale reconstruction in image analysis: Applications and efficient algorithms," *IEEE Trans. Image process.*, vol. 2, no. 2, pp. 176–201, Apr. 1993.
- [46] Z. Zhen, L. Quackenbush, and L. Zhang, "Impact of tree-oriented growth order in marker-controlled region growing for individual tree crown delineation using airborne laser scanner (ALS) data," *Remote Sens.*, vol. 6, no. 1, pp. 555–579, 2014.
- [47] E. Sibona *et al.*, "Direct measurement of tree height provides different results on the assessment of LiDAR accuracy," *Forests*, vol. 8, no. 1, pp. 7–18, 2017.
- [48] S. Gupta, H. Weinacker, and B. Koch, "Comparative analysis of clustering-based approaches for 3-D single tree detection using airborne fullwave LiDAR data," *Remote Sens.*, vol. 2, no. 4, pp. 968–989, 2010.

- [49] J.-M. Monnet, E. Mermin, J. Chanussot, and F. Berger, "Tree top detection using local maxima filtering: A parameter sensitivity analysis," in *Proc. 10th Int. Conf. LiDAR App. Assessing Forest Ecosystems (Silvilaser 2010)*, Sep. 2010, Freiburg, Germany. 9 p. hal-00523245.
- [50] M. Dalponte, L. Frizzera, and D. Gianelle, "Estimation of forest attributes at single tree level using hyperspectral and ALS data," in *Proc. ForestSAT Conf.*, 2014.



**Juntao Yang** received the master's degree in LiDAR technology in 2017 from the China University of Geosciences, Beijing, China, where he is currently working toward the Ph.D. degree at the School of Land Science and Technology.

He has authored more than ten referred journal and conference publications. His research interests include LiDAR data processing, computer vision, and lunar structure recognition and analysis.



**Zhizhong Kang** received the Ph.D. degree in photogrammetry and remote sensing from Wuhan University, Hubei, China, in 2004.

From 2006 to 2008, he was a Postdoctoral Researcher with the Delft University of Technology, The Netherlands. He is currently a Full Professor and the Vice Dean of the School of Land Science and Technology, China University of Geosciences, Beijing, China. He has authored more than 100 referred journal and conference publications. His research interests include digital photogrammetry, Li-

DAR data processing, indoor modeling and navigation, and Planetary remote sensing.

Dr. Kang was the Chair of ISPRS WG IV/5: Indoor/Outdoor seamless modelling, LBS, mobility. He received the 2015 ERDAS Award for Best Scientific Paper in Remote Sensing by the American Society for Photogrammetry and Remote Sensing.



**Sai Cheng** received the B.S. degree in geomatic engineering in 2017 from the China University of Geosciences, Beijing, China, where he is currently working toward the M.S. degree at the School of Land Science and Technology.

He has authored two referred journal and conference publications. His research interests include LiDAR data processing and visual SLAM.



**Zhou Yang** received the B.S. degree in geomatics in 2019 from the China University of Geosciences, Beijing, China, where he is currently working toward the M.S. degree in LiDAR technology at the School of Land Science and Technology.

His research interests include LiDAR data processing and 3-D building reconstruction.



**Perpetual Hope Akwensi** received the B.S. degree in geomatic engineering from the Faculty of Mineral Resource Technology, University of Mines and Technology, Tarkwa, Ghana, in 2014. She is currently working toward the M.S. degree in remote sensing and geo-information engineering at the China University of Geosciences, Beijing, China.

Since 2017, she has been doing research on the processing of 3-D LiDAR point cloud data. Her research interests include remotely sensed image processing, 3-D point cloud segmentation and classification, and machine learning.